



# Synthesis of ternary zinc spinel oxides and their application in the photodegradation of organic pollutant

Chayene G. Anchieta<sup>a</sup>, Daniela Sallet<sup>a</sup>, Edson L. Foletto<sup>a,\*</sup>, Syllos S. da Silva<sup>b</sup>, Osvaldo Chiavone-Filho<sup>b</sup>, Claudio A.O. do Nascimento<sup>c</sup>

<sup>a</sup>Department of Chemical Engineering, Federal University of Santa Maria, 97105-900 Santa Maria, Brazil

<sup>b</sup>Department of Chemical Engineering, Federal University of Rio Grande do Norte, 59066-800 Natal, Brazil

<sup>c</sup>Department of Chemical Engineering, University of São Paulo, 05508-900 São Paulo, Brazil

Received 24 May 2013; received in revised form 16 July 2013; accepted 19 August 2013

Available online 31 August 2013

## Abstract

Ternary zinc spinel oxides such as  $Zn_2SnO_4$ ,  $ZnAl_2O_4$  and  $ZnFe_2O_4$  were synthesized and characterized, and their activities in the photodegradation of phenol molecules were investigated.  $Zn_2SnO_4$ ,  $ZnAl_2O_4$  and  $ZnFe_2O_4$  powders were synthesized by hydrothermal, metal–chitosan complexation and solvothermal routes, respectively. The face-centered cubic spinel structure of each material was confirmed by powder X-ray diffractometry (XRD) and its porous structure by  $N_2$  adsorption–desorption isotherms. The characterization of spinels was complemented with Fourier transform infrared spectroscopy (FTIR) and X-rays fluorescence (XRF), revealing the formation of spinel structures with high purity. The photocatalytic activity in the degradation of phenol was observed only with  $Zn_2SnO_4$  oxide. Mineralization degree of phenol molecules by  $Zn_2SnO_4$  photocatalyst determined by total organic carbon analysis (TOC) reached 80% at 360 min under sunlight.

© 2013 Elsevier Ltd and Techna Group S.r.l. All rights reserved.

**Keywords:** Synthesis;  $Zn_2SnO_4$ ;  $ZnAl_2O_4$ ;  $ZnFe_2O_4$ ; Photocatalysis

## 1. Introduction

Zinc aluminate ( $ZnAl_2O_4$ ) and zinc ferrite ( $ZnFe_2O_4$ ) are ternary oxide semiconductors of the form  $AB_2O_4$ , while zinc stannate ( $Zn_2SnO_4$ ) has the chemical formula  $A_2BO_4$ , where A represents a divalent metallic cation that usually occupies a tetrahedral site and B represents trivalent or tetravalent metallic cations that normally occupy the octahedral sites of a cubic structure [1,2]. As important semiconductor materials these three spinels have received much more attention recently. Due to the high electron mobility, high electrical conductivity and attractive optical properties, the  $Zn_2SnO_4$  semiconductor is suitable for a wide range of applications such as solar cells, sensors for the detection of humidity and various combustible gases, and negative electrode material for Li-ion battery [2].  $ZnAl_2O_4$  is of interest due to its combination of desirable properties such as high mechanical resistance, high thermal

stability, low temperature sinterability, low surface acidity and better diffusion. Therefore, it is used as high temperature ceramic material, optical coating or host matrix but most importantly as catalyst or catalyst support [3,4].  $ZnFe_2O_4$  has attracted significant research interest based on its magnetic and electromagnetic properties [5–7]. In addition, zinc ferrite shows potentially wide applications in photo induced electron transfer, photo-electrochemical cells and photo-chemical hydrogen production [8]. Ternary semiconductor oxides have also been used as catalysts and catalyst supports in several reactions [9–13], but its application in the field of the photocatalysis yet is limited. They have been applied more on degrading of different organic dyes [1,14–16]. However, the use of these spinel oxides as photocatalysts in the degradation of phenol has still been under explored. To the best of our knowledge, the evaluation of the photocatalytic activity of ternary zinc spinel oxides in the degradation of phenol under sunlight is scarce. Phenol is widely used in many petrochemical industries and petroleum refineries as well as chemical and pharmaceutical industries. Phenol pollution

\*Corresponding author. Tel.: +55 55 3220 8448; fax: +55 55 3220 8030.

E-mail address: [efoletto@gmail.com](mailto:efoletto@gmail.com) (E.L. Foletto).

inhibits or even eliminates micro-organisms in biological wastewater treatment plant [17].

In this context, the aim of this work was to evaluate the photocatalytic activity of three zinc spinel oxides in the degradation of phenol molecules under solar irradiation. The oxides were synthesized by different methods and its physical properties were investigated by the characterization techniques powder X-ray diffraction (XRD), infrared spectroscopy (FTIR), X-rays fluorescence (XRF) and  $N_2$  adsorption–desorption isotherms.

## 2. Materials and methods

### 2.1. Synthesis of the spinel photocatalysts

#### 2.1.1. Synthesis of $Zn_2SnO_4$

The zinc acetate ( $Zn(CH_3COO)_2 \cdot 2H_2O$ ) aqueous solution (12.85 g in 59 mL of water) was added into the tin tetrachloride ( $SnCl_4 \cdot 5H_2O$ ) aqueous solution (8.80 g in 50 mL of water) slowly. The NaOH aqueous solution (5 M) was added dropwise into the mixture under magnetic stirring, until the solution reach pH 7.5. The final mixture was charged into a PTFE-lined stainless autoclave and the hydrothermal reaction was carried out at 200 °C for 10 h. Subsequently, the autoclave was allowed to cool naturally. The precipitate was filtered, washed with distilled water, and dried at 100 °C for 12 h.

#### 2.1.2. Synthesis of $ZnAl_2O_4$

the preparation of  $ZnAl_2O_4$  powder by metal–chitosan complexation route was similar to that described in previous works, but for the synthesis of magnesium aluminate ( $MgAl_2O_4$ ) [18,19]. For the  $ZnAl_2O_4$  synthesis, 9.84 g of chitosan polymer [ $(C_6H_{11}O_4N)_n$ ] (Purifarma, Brazil) were dissolved in 334 mL of acetic acid solution (5% v/v), 11.88 g of  $Zn(NO_3)_2 \cdot 6H_2O$  were dissolved in 20 mL distilled water and 31.5 g of  $Al(NO_3)_3 \cdot 9H_2O$  were dissolved in 30 mL distilled water. The Zn and Al aqueous solutions were then added to the polymer solution under magnetic stirring. The Zn–Al–chitosan solution was added dropwise with a peristaltic pump to a  $NH_4OH$  solution (50%, v/v) under vigorous stirring. After adding the solutions, the system was kept under stirring for 3 h to complete the gelification process. The product was separated from the solution and further dried at ambient temperature for 24 h. The material was then treated in an oxidizing atmosphere (air) at the temperature of 750 °C, for 5 h, to form the spinel phase.

#### 2.1.3. Synthesis of $ZnFe_2O_4$

In order to obtain the  $ZnFe_2O_4$  powder, stoichiometric amounts of zinc nitrate (3 mmol of  $Zn(NO_3)_2 \cdot 6H_2O$ ) and iron nitrate (6 mmol of  $Fe(NO_3)_3 \cdot 9H_2O$ ) were dissolved in ethylene glycol (90 mL), followed by the addition of 45 mmol of sodium acetate ( $CH_3COONa$ ) under magnetic stirring. After continuous stirring for 45 min, a homogeneous solution was obtained. The final solution was charged into a PTFE-lined stainless autoclave and the solvothermal reaction was carried out at 200 °C for 15 h. The product was then filtered and

washed several times with distilled water and absolute ethanol, and subsequently dried at 110 °C for 24 h.

### 2.2. Characterization of the spinel photocatalysts

The zinc spinel oxides were characterized by X-ray diffractometry (XRD) (equipment Bruker D8 Advance, with  $Cu K\alpha$  radiation). The average size of the crystallite of each oxide was determined through the Scherrer equation [20]:  $D = K\lambda / (h_{1/2} \cdot \cos \Theta)$ , where  $D$  is the average crystallite size,  $K$  the Scherrer constant (0.9),  $\lambda$  the wavelength of incident X-rays (0.15405 nm),  $h_{1/2}$  the width at half height of the most intense diffraction peak and  $\Theta$  corresponds to the peak position. FTIR spectra were recorded on a PerkinElmer FTIR Spectrum spectrophotometer in the region of 375–4000  $cm^{-1}$ , using KBr pellets. The Brunauer–Emmett–Teller (BET) surface area measurement was carried out by  $N_2$  adsorption–desorption at 77 K using ASAP 2000 instrument, in the range relative pressure ( $P/P_0$ ) of 0 to 0.99. Chemical composition of the oxide powders was determined by X-ray fluorescence (EDX-750, Shimadzu) spectrometry.

### 2.3. Photocatalytic activity

Three photochemical reactors ( $\varnothing_{int.} = 10$  cm) of 200 mL capacity, irradiated by sunlight, were used simultaneously in the photocatalytic experiments, according to the scheme of the reaction system seen in Fig. 1. The experiments under sunlight were carried out between 8:30 am and 14:30 pm during the month of January/2013 (summer season) at Natal City (05° 47' 42" S and 35° 12' 34" W), located in a northeastern state of Brazil. For all tests, 0.15 g of each spinel oxide was added to 150 mL of the aqueous solution of phenol at an initial concentration of 20  $mg L^{-1}$ . The pH of the suspension was not adjusted (initial pH=6.3). Prior to irradiation, the resulting suspensions were stirred continuously at constant temperature (25 °C) in the dark to achieve the adsorption equilibrium of phenol on each catalyst. The suspensions were then irradiated using sunlight under continuous stirring. Samples were periodically taken from the reactors, and filtered before being

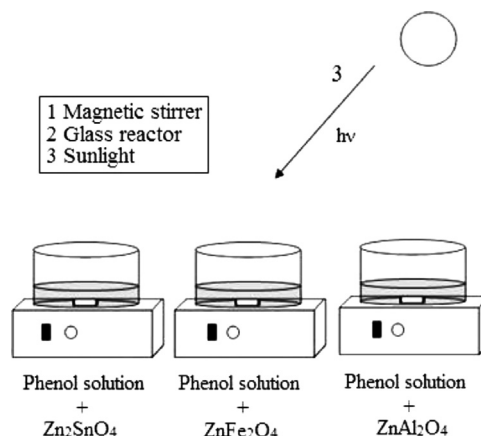


Fig. 1. Apparatus used in the photocatalytic experiments under solar irradiation.

subjected to a UV–vis spectrophotometer (Varian 50), at  $\lambda_{max}=270$  nm. The photodegradation performance of phenol was defined as [21]:

$$\% \text{ REM} = (A_0 - A_t) / A_0 \times 100 \quad (1)$$

where  $A_0$  is the initial absorbance of the synthetic solution and  $A_t$  is the absorbance at reaction time  $t$ .

The decrease in total organic carbon (TOC), which indicated the mineralization of phenol, was determined using a TOC analyzer (Shimadzu 5000A, Japan). The degree of mineralization was calculated based on the TOC percent removal rate, according to expression:

$$\% \text{ Mineralization} = (\text{TOC}_0 - \text{TOC}_t) / \text{TOC}_0 \times 100 \quad (2)$$

where  $\text{TOC}_0$  is the initial TOC of the synthetic solution and  $\text{TOC}_t$  is its value at reaction time  $t$ . All experiments were carried out in duplicate and only the mean values were reported.

### 3. Results and discussion

Fig. 2 shows the XRD patterns of ternary oxide samples prepared in this work. All the diffraction peaks for the three oxides can be indexed to a cubic structure, which represents a good agreement with the value found in the literature (JCPDS card no. 01-070-6393, JCPDS card no. 74-2184 and JCPDS card no. 05-0669, for the  $\text{ZnFe}_2\text{O}_4$ ,  $\text{Zn}_2\text{SnO}_4$  and  $\text{ZnAl}_2\text{O}_4$  samples, respectively). For the  $\text{ZnAl}_2\text{O}_4$  oxide, the characteristic peaks at  $2\Theta$  of  $31.2^\circ$ ,  $36.75^\circ$ ,  $44.7^\circ$ ,  $49.1^\circ$ ,  $55.6^\circ$  and  $59.3^\circ$  are corresponding to (220), (311), (400), (331), (422) and (511) diffraction planes, respectively. The diffraction

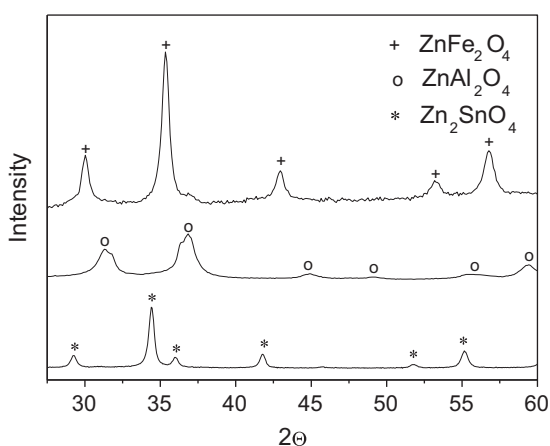


Fig. 2. XRD patterns of the different zinc spinel oxides.

peaks at  $2\Theta$  values of  $29.25^\circ$ ,  $34.43^\circ$ ,  $35.96^\circ$ ,  $41.79^\circ$ ,  $51.74^\circ$  and  $55.14^\circ$  can be ascribed to the reflection of (220), (311), (222), (400), (422) and (511) planes of the  $\text{Zn}_2\text{SnO}_4$  spinel, respectively. For the  $\text{ZnFe}_2\text{O}_4$  oxide, the characteristic peaks at  $2\Theta$  of  $30.05^\circ$ ,  $35.36^\circ$ ,  $42.78^\circ$ ,  $52.96^\circ$  and  $56.78^\circ$  are corresponding to (220), (311), (400), (422) and (511) diffraction planes, respectively. No additional peak of the other phase was observed in the XRD patterns, showing that the ternary oxides consisted of single-phase. It should be observed that the  $\text{ZnAl}_2\text{O}_4$  sample showed wider peaks than that of the  $\text{ZnFe}_2\text{O}_4$  and  $\text{Zn}_2\text{SnO}_4$  oxides, indicating a small crystallite size. Crystallite size of synthesized powders (shown in Table 1), based on Scherrer equation, was estimated at 7.30, 15.79 and 17.10 nm, for the  $\text{ZnAl}_2\text{O}_4$ ,  $\text{ZnFe}_2\text{O}_4$  and  $\text{Zn}_2\text{SnO}_4$  oxides, respectively.

Fig. 3 shows the FTIR spectrum of spinel oxides prepared in this work. It can be observed in figure two main broad bands in the range  $375\text{--}750\text{ cm}^{-1}$  for all zinc spinel oxides. The band around  $375\text{--}500\text{ cm}^{-1}$  corresponds to interaction between metal and oxygen in the octahedral site in the crystal lattice, and the band around  $550\text{--}750\text{ cm}^{-1}$  corresponds to interaction between metal and oxygen in the tetrahedral site. In the  $\text{Zn}_2\text{SnO}_4$  spinel, the band observed at  $570\text{ cm}^{-1}$  can be assigned to Zn–O bonds at the tetrahedral site, and the band observed at  $420\text{ cm}^{-1}$  involves the Sn–O bonds in octahedral site. For the  $\text{ZnAl}_2\text{O}_4$  solid, vibration at  $680\text{ cm}^{-1}$  is typical of Zn–O bonds, while that the vibration at  $530\text{ cm}^{-1}$  is characteristic of Al–O bonds. In the case of  $\text{ZnFe}_2\text{O}_4$  oxide, the band at  $570\text{ cm}^{-1}$  and  $420\text{ cm}^{-1}$  are assigned to interactions of Zn–O bonds in tetrahedral positions and the Fe–O bonds in octahedral positions, respectively. The results obtained in the analysis of FTIR confirm the formation of spinel structures and corroborate the results obtained in the XRD analysis.

Nitrogen adsorption–desorption isotherm measurements were carried out to evaluate the specific surface areas (Fig. 4a) as well as the average pore size distributions (Fig. 4b) of zinc spinel oxides. The isotherms of all zinc spinels prepared in this work can be classified as type IV, according to the IUPAC classification [22], indicating predominantly mesoporous structure characteristics. The mesoporous structure of samples was confirmed by analysis of average pore size distribution (Fig. 4b), which shows the spectra of pore diameter distribution with defined maxima in mesoporous region ( $2\text{ nm} < \text{pore diameter} < 50\text{ nm}$ ) for all the samples. The pore size distribution curves display a narrow unimodal distribution for the  $\text{Zn}_2\text{SnO}_4$  and  $\text{ZnAl}_2\text{O}_4$  oxides, and wide unimodal distribution for  $\text{ZnFe}_2\text{O}_4$  spinel. The surface areas of oxides were measured from the linear

Table 1  
Crystallite size, BET surface area and pore parameters of the different zinc spinel oxides.

Samples	Crystallite size (nm)	Surface area ( $\text{m}^2\text{ g}^{-1}$ )	Total pore volume ( $\text{cm}^3\text{ g}^{-1}$ )	Average pore size (nm)
$\text{ZnFe}_2\text{O}_4$	15.79	58.96	0.185	18.72
$\text{ZnAl}_2\text{O}_4$	7.30	158.10	0.302	7.44
$\text{Zn}_2\text{SnO}_4$	17.10	42.91	0.191	4.11

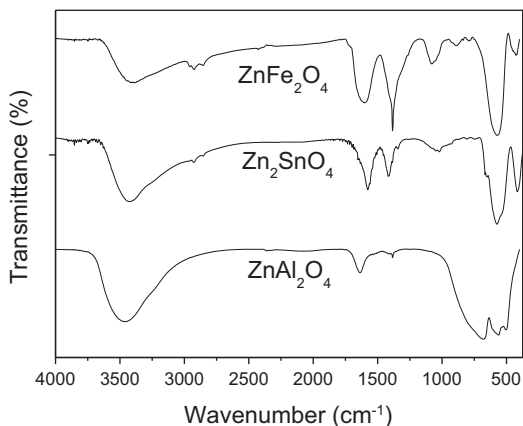


Fig. 3. FTIR spectra of different zinc spinel oxides.

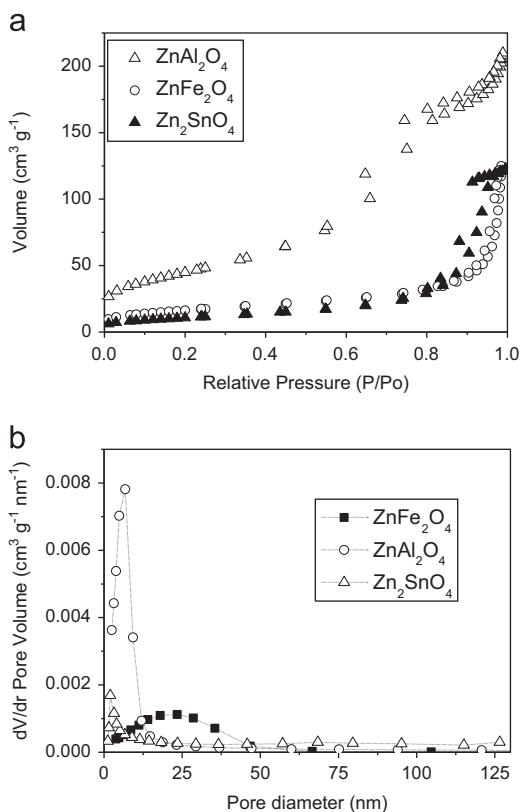


Fig. 4. (a) Nitrogen adsorption–desorption isotherms and (b) pore size distribution of different zinc spinel oxides.

region of the plot ranging from  $P/P_0=0.05$  to  $P/P_0=0.30$ , and the results are shown in Table 1.

Table 1 summarizes the results of physical properties of zinc spinel oxides. The surface area of  $ZnAl_2O_4$  was higher than these of other oxides, however, the pore size was smaller. High surface area and pore size are essential characteristics for catalytic purpose.

Chemical compositions determined by X-rays fluorescence technique for the powders are listed in Table 2. The results reveal that only minor undesirable substances remained in the synthesized powders.  $ZnAl_2O_4$  powders contains less than 0.4 wt% impurities, which were nickel, iron, calcium and

sulfur, whereas that the  $Zn_2SnO_4$  oxide contains less than 0.2 wt% impurities, such as calcium and nickel. Yet  $ZnFe_2O_4$  powders contains nickel and sulfur as impurities, corresponding to about 0.15 wt%. These impurities may be present in the salts used as reagents in the synthesis of the spinel oxides, i.e., zinc nitrate, aluminum nitrate, zinc acetate, tin tetrachloride and iron nitrate. Therefore, the  $ZnAl_2O_4$ ,  $ZnFe_2O_4$  and  $Zn_2SnO_4$  powders obtained by the presented method in this work were of high grade of purity.

The degradation of the phenol molecules was negligible by direct photolysis (with sunlight only) as well as by the use of  $ZnFe_2O_4$  and  $ZnAl_2O_4$  oxides as photocatalysts.  $ZnFe_2O_4$  presented less than 5% of phenol degradation after 240 min of reaction while  $ZnAl_2O_4$  did not present any photocatalytic activity. A significant degradation of the phenol was only observed with the presence of  $Zn_2SnO_4$  photocatalyst and sunlight. In addition, the phenol adsorption carried out in the dark before photocatalytic process was negligible, indicating that the adsorption step do not contribute to the phenol removal from aqueous solution. Although the  $ZnAl_2O_4$  photocatalysts has shown photocatalytic activity in degradation of dye molecules under sunlight [16], and  $ZnFe_2O_4$  has presented activity for the degrading of phenol under artificial UV light [23,24], both oxides did not show activity for degrading of phenol under solar irradiation in this work. This indicates that the intensity of sunlight may be insufficient to cause excitation of both semiconductors used as photocatalysts, which is necessary for that the photocatalysis reaction to occur. The degradation efficiency of each photocatalyst also depends on the organic pollutant type and its concentration that will be degraded. Fig. 5 shows the degradation of phenol as well as the degree of mineralization in terms of TOC removal with the use of the  $Zn_2SnO_4$  sample only. After 240 min of exposition to solar irradiation this oxide was able to degrade 98% of the phenol. However, the mineralization degree reached after 240 min under solar irradiation was 60%, reaching 80% after 360 min of reaction time. The TOC removal usually takes longer time than that for the removal of pollutant organic molecules, as also found in another researches [25,26].

Several photodegradation reactions of organic pollutants follow first-order kinetics [27–29], which the photodegradation rate ( $r$ ) in this case can be expressed as first-order with respect to the disappearance of phenol molecules, i.e.,

$$r = -d[C]/dt = k[C] \quad (3)$$

The integrated reaction rate gives:

$$\ln[C] = -kt + \ln[C_0] \quad (4)$$

which is usually written in the exponential form:

$$C/C_0 = \exp(-kt) \quad (5)$$

The linearized form of above equation can be written as follows:

$$\ln(C/C_0) = -kt \quad (6)$$

Therefore, the photocatalytic process of phenol removal at sunlight follows first-order kinetics according to the Eq. (4), where  $C_0$  is the initial concentration of phenol solution,  $C$  is

Table 2  
Chemical composition of the synthesized spinels, expressed in wt%.

Sample	Constituent				
ZnAl <sub>2</sub> O <sub>4</sub>	ZnAl <sub>2</sub> O <sub>4</sub> (99.62)	NiO (0.18)	Fe <sub>2</sub> O <sub>3</sub> (0.10)	CaO (0.05)	SO <sub>3</sub> (0.05)
Zn <sub>2</sub> SnO <sub>4</sub>	Zn <sub>2</sub> SnO <sub>4</sub> (99.81)	NiO (0.14)	–	CaO (0.05)	–
ZnFe <sub>2</sub> O <sub>4</sub>	ZnFe <sub>2</sub> O <sub>4</sub> (99.86)	NiO (0.09)	–	–	SO <sub>3</sub> (0.05)

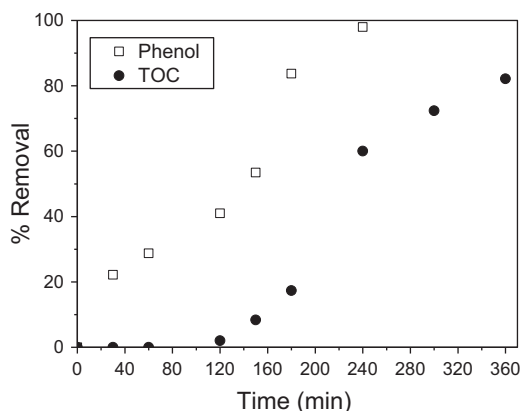


Fig. 5. Phenol and TOC removal as a function of time by the Zn<sub>2</sub>SnO<sub>4</sub> photocatalyst.

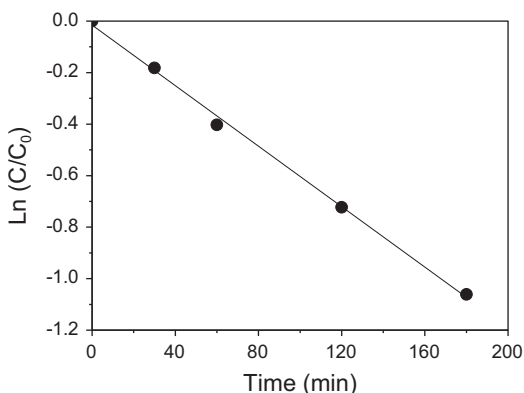


Fig. 6. Kinetics of phenol photodegradation reaction obtained by the Zn<sub>2</sub>SnO<sub>4</sub> photocatalyst.

the concentration at time  $t$ , and  $k$  is the reaction rate constant of photocatalysis process. The relative concentration  $C/C_0$  also can be determined by ratio  $A/A_0$ , where  $A$  and  $A_0$  were defined previously. The straight line (see Fig. 6) indicates first-order reaction and the slope of this line corresponds to the reaction rate constant ( $k$ ), which was of  $k = 5.8 \times 10^{-3} \text{ min}^{-1}$ .

#### 4. Conclusions

Zinc spinel oxides particles were successfully synthesized by hydrothermal, metal–chitosan complexation and solvothermal methods, respectively. All the samples presented crystal-line structure, with high purity and predominantly mesoporous, but in terms of photocatalytic activity, Zn<sub>2</sub>SnO<sub>4</sub> oxide was the only one that showed activity in the degradation of phenol

molecules under solar irradiation reaching removal of 100% at 240 min of reaction. At 360 min under sunlight the mineralization of phenol was of 80%, which demonstrate the potential of Zn<sub>2</sub>SnO<sub>4</sub> oxide as photocatalyst in the removal of phenol pollutant in aqueous solution under sunlight.

#### Acknowledgments

The authors thank the CAPES (Brazil), for the financial support.

#### References

- [1] E.L. Foletto, S.L. Jahn, R.F.P.M. Moreira, Hydrothermal preparation of Zn<sub>2</sub>SnO<sub>4</sub> nanocrystals and photocatalytic activity in the degradation of leather dye, *Journal of Applied Electrochemistry* 40 (2010) 59–63.
- [2] S. Baruah, J. Dutta, Zinc stannate nanostructures:hydrothermal synthesis, *Science and Technology of Advanced Materials* (2011) <http://dx.doi.org/10.1088/1468-6996/12/1/013004>.
- [3] M. Zawadzki, Synthesis of nanosized and microporous zinc aluminate spinel by microwave assisted hydrothermal method (microwave–hydrothermal synthesis of ZnAl<sub>2</sub>O<sub>4</sub>), *Solid State Sciences* 8 (2006) 14–18.
- [4] H. Dixit, N. Tandon, S. Cottenier, R. Saniz, D. Lamoen, B. Partoens, V. Van Speybroeck, M. Waroquier, Electronic structure and band gap of zinc spinel oxides beyond LDA: ZnAl<sub>2</sub>O<sub>4</sub>, ZnGa<sub>2</sub>O<sub>4</sub> and ZnIn<sub>2</sub>O<sub>4</sub>, *New Journal of Physics* (2011) <http://dx.doi.org/10.1088/1367-2630/13/6/063002>.
- [5] W. Schiessl, W. Potzel, H. Karzel, M. Steiner, G.M. Kalvius, A. Martin, M.K. Krause, I. Halevy, J. Gal, W. Schäfer, G. Will, M. Hillberg, R. Wäppling, Magnetic properties of the ZnFe<sub>2</sub>O<sub>4</sub> spinel, *Physical Review B* 53 (1996) 9143–9152.
- [6] C. Yao, Q. Zeng, G.F. Goya, T. Torres, J. Liu, H. Wu, M. Ge, Y. Zeng, Y. Wang, J.Z. Jiang, ZnFe<sub>2</sub>O<sub>4</sub> nanocrystals: Synthesis and magnetic properties, *Journal of Physical Chemistry C* 111 (2007) 12274–12278.
- [7] S.A. Popescu, P. Vlazan, Ş. Novaconi, I. Grozescu, P.V. Nojinger, Electromagnetic behavior of zinc ferrite obtained by a coprecipitation technique, *U.P.B Scientific Bulletin, Series C* 73 (2011) 247–256.
- [8] N.M. Deraz, A. Alarifi, Microstructure and magnetic studies of zinc ferrite nano-particles, *International Journal of Electrochemical Science* 7 (2012) 6501–6511.
- [9] J.A. Toledo-Antonio, N. Nava, M. Martínez, X. Bokhimi, Correlation between the magnetism of non-stoichiometric zinc ferrites and their catalytic activity for oxidative dehydrogenation of 1-butene, *Applied Catalysis A: General* 234 (2002) 137–144.
- [10] M. Vijayaraj, C.S. Gopinath, On the active spacer and stabilizer role of Zn in Cu<sub>1-x</sub>Zn<sub>x</sub>Fe<sub>2</sub>O<sub>4</sub> in the selective mono-N-methylation of aniline: XPS and catalysis study, *Journal of Catalysis* 241 (2006) 83–95.
- [11] M. Lenarda, M. Casagrande, E. Moretti, L. Storaro, R. Frattini, S. Polizzi, Selective catalytic low pressure hydrogenation of acetophenone on Pd/ZnO/ZnAl<sub>2</sub>O<sub>4</sub>, *Catalysis Letters* 114 (2007) 79–84.
- [12] M. Zawadzki, W. Staszak, F.E.L. Suárez, M.J.I. Gómez, A.B. López, Preparation, characterisation and catalytic performance for soot oxidation of copper-containing ZnAl<sub>2</sub>O<sub>4</sub> spinels, *Applied Catalysis A: General* 371 (2009) 92–98.

- [13] A.E. Galetti, M.F. Gomez, L.A. Arrúa, M.C. Abello, Ni catalysts supported on modified  $\text{ZnAl}_2\text{O}_4$  for ethanol steam reforming, *Applied Catalysis A: General* 380 (2010) 40–47.
- [14] G. Fan, Z. Gu, L. Yang, F. Li, Nanocrystalline zinc ferrite photocatalysts formed using the colloid mill and hydrothermal technique, *Chemical Engineering Journal* 155 (2009) 534–541.
- [15] Z. Jia, D. Ren, Y. Liang, R. Zhu, A new strategy for the preparation of porous zinc ferrite nanorods with subsequently light-driven photocatalytic activity, *Materials Letters* 65 (2011) 3116–3119.
- [16] E.L. Foletto, S. Battiston, J.M. Simões, M.M. Bassaco, L.S.F. Pereira, É.M.M. Flores, E.I. Müller, Synthesis of  $\text{ZnAl}_2\text{O}_4$  nanoparticles by different routes and the effect of its pore size on the photocatalytic process, *Microporous and Mesoporous Materials* 163 (2012) 29–33.
- [17] N.A. Laoufi, D. Tassalit, F. Bentahar, The degradation of phenol in water solution by  $\text{TiO}_2$  photocatalysis in a helical reactor, *Global NEST Journal* 10 (2008) 404–418.
- [18] G.D.B. Nuernberg, E.L. Foletto, L.F.D. Probst, C.E.M. Campos, C.E.M., N.L.V. Carreño, M.A. Moreira, A novel synthetic route for magnesium aluminate ( $\text{MgAl}_2\text{O}_4$ ) particles using metal–chitosan complexation method, *Chemical Engineering Journal* (2012) 211–214 (193–194).
- [19] G.D.B. Nuernberg, E.L. Foletto, L.F.D. Probst, N.L.V. Carreño, M. A. Moreira,  $\text{MgAl}_2\text{O}_4$  spinel particles prepared by metal–chitosan complexation route and used as catalyst support for direct decomposition of methane, *Journal of Molecular Catalysis A: Chemical* 370 (2013) 22–27.
- [20] B.D. Cullity, S.R. Stock, *Elements of X-Ray Diffraction*, 3rd Ed., Prentice-Hall Inc., New Jersey, 2001.
- [21] G.C. Collazzo, E.L. Foletto, S.L. Jahn, M.A. Villetti, Degradation of Direct Black 38 dye under visible light and sunlight irradiation by N-doped anatase  $\text{TiO}_2$  as photocatalyst, *Journal of Environmental Management* 98 (2012) 107–111.
- [22] International Union of Pure and Applied Chemistry, IUPAC, *Pure and Applied Chemistry*, vol. 57, 1985 p. 603.
- [23] M.A. Valenzuela, P. Bosch, J. Jiménez-Becerrill, O. Quiroz, A.I. Pérez, Preparation, characterization and photocatalytic activity of  $\text{ZnO}$ ,  $\text{Fe}_2\text{O}_3$  and  $\text{ZnFe}_2\text{O}_4$ , *Journal of Photochemistry and Photobiology A: Chemistry* 148 (2002) 177–182.
- [24] S.-Wen Cao, Y.-Jie Zhu, G.-Feng Cheng, Y.-Hong Huang,  $\text{ZnFe}_2\text{O}_4$  nanoparticles: Microwave-hydrothermal ionic liquid synthesis and photocatalytic property over phenol, *Journal of Hazardous Materials* 171 (2009) 431–435.
- [25] E.L. Foletto, J.M. Simões, M.A. Mazutti, S.L. Jahn, E.I. Muller, L.S. F. Pereira, E.M.M. Flores, Application of  $\text{Zn}_2\text{SnO}_4$  photocatalyst prepared by microwave-assisted hydrothermal route in the degradation of organic pollutant under sunlight, *Ceramics International* 39 (2013) 4569–4574.
- [26] P. Sathishkumar, R. Sweena, J.J. Wu, S. Anandan, Synthesis of CuO-ZnO nanophotocatalyst for visible light assisted degradation of a textile dye in aqueous solution, *Chemical Engineering Journal* 171 (2011) 136–140.
- [27] L.J.V. Silva, E.L. Foletto, L.S. Dorneles, D.S. Paz, T.S. Frantz, A. Gundel, ZnO electrodeposition onto gold from recordable compact discs and its use as photocatalyst under solar irradiation, *Brazilian Society of Chemical Engineering* 30 (2013) 155–158.
- [28] R.-Chi Wang, C.-Wen Yu, Phenol degradation under visible light irradiation in the continuous system of photocatalysis and sonolysis, *Ultrasonics Sonochemistry* 20 (2013) 553–564.
- [29] E.L. Foletto, S. Battiston, G.C. Collazzo, M.M. Bassaco, M.A. Mazutti, Degradation of leather dye using  $\text{CeO}_2\text{-SnO}_2$  nanocomposite as photocatalyst under sunlight, *Water, Air, and Soil Pollution* 223 (2012) 5773–5779.